Social Network Analysis and Mining (2022) 12:13
https://doi.org/10.1007/s13278-021-00839-8

ORIGINAL ARTICLE

Natural disaster evacuation modeling: the dichotomy of fear of crime and social influence

Chris J. Kuhlman[1] · Achla Marathe[2] · Anil Vullikanti[3] · Nafisa Halim[4] · Pallab Mozumder[5]

Received: 31 December 2020 / Revised: 30 October 2021 / Accepted: 31 October 2021

Abstract
Neighborhood effects have an important role in evacuation decision-making by a family. Owing to peer influence, neighbors evacuating can motivate a family to evacuate. Paradoxically, if a lot of neighbors evacuate, then the likelihood of an individual or family deciding to evacuate decreases, for fear of crime and looting. Such behavior cannot be captured using standard models of contagion spread on networks, e.g., threshold, independent cascade, and linear threshold models. Here, we propose a new threshold-based graph dynamical system model, 2MODE-THRESHOLD, which captures this dichotomy. We study theoretically the dynamical properties of 2MODE-THRESHOLD in different networks, and find significant differences from a standard threshold model. We build and characterize small world networks of Virginia Beach, VA, where nodes are geolocated families (households) in the city and edges are interactions between pairs of families. We demonstrate the utility of our behavioral model through agent-based simulations on these small world networks. We use it to understand evacuation rates in this region, and to evaluate the effects of modeling parameters on evacuation decision dynamics. Specifically, we quantify the effects of (1) network generation parameters, (2) stochasticity in the social network generation process, (3) model types (2MODE-THRESHOLD vs. standard threshold models), (4) 2MODE-THRESHOLD model parameters, (5) and initial conditions, on computed evacuation rates and their variability. An illustrative example result shows that the absence of looting effect can overpredict evacuation rates by as much as 50%.

✉ Chris J. Kuhlman
cjk8gx@virginia.edu

Achla Marathe
achla@virginia.edu

Anil Vullikanti
vsakumar@virginia.edu

Nafisa Halim
nhalim@bu.edu

Pallab Mozumder
mozumder@fiu.edu

[1] Biocomplexity Institute and Initiative, University of Virginia, Charlottesville, VA, USA

[2] Biocomplexity Institute and Initiative, Department of Public Health Sciences, University of Virginia, Charlottesville, VA, USA

[3] Biocomplexity Institute and Initiative, Department of Computer Science, University of Virginia, Charlottesville, VA, USA

[4] Department of Global Health, Boston University School of Public Health, Boston, MA, USA

[5] Department of Earth and Environment and Department of Economics, Florida International University, Miami, FL, USA

1 Introduction

1.1 Background

Extreme weather events displaced seven million people from their homes just in the first 6 months of 2019 (Sengupta 2019). With the rise in global warming, the frequency of these events is increasing and they are also becoming more damaging (Coumou and Rahmstorf 2012). Just in 2017–2018, there were 24 major events. In 2017, there was a total of 16 weather events that together costed over $306 billion, according to NOAA. In 2018, there were eight hurricanes, out of which two were category three or higher and caused more than $50 billion in damages. As of this writing, the 2020 hurricane season, well underway, is anticipated to have near-record-breaking counts, with ten total hurricanes including four major ones (Saunders and Lea, August 2020).

Published online: 29 November 2021

1.2 Motivation for studying fear of looting in natural disaster contexts

Timely evacuation is the only action that can reduce risk in many of these events. Although more people are exposed to these weather events, technological improvements in weather prediction, early warning systems, emergency management, and information sharing through social media, have helped keep the number of fatalities fairly low. During Hurricane Fani (Kumar 2019), a record 3.4 million people were evacuated in India and Bangladesh and fewer than 100 fatalities were recorded (Sengupta 2019). However, in many disaster events, e.g., Hurricane Sandy, the fraction of people who evacuated has been much lower than what local governments would like.

The decision to evacuate or not is a very complex one and depends on a large number of social, demographic, familial, and psychological factors, including forecasts, warnings, and risk perceptions (Madireddy et al. 2015; Yang et al. 2019; Hasan and Ukkusuri 2011; Widener et al. 2013; Halim and Mozumder 2020). Two specific factors have been shown to have an important effect on evacuation decisions. First, peer effects, i.e., whether neighbors and others in the community have evacuated. Up to a point, this has a positive impact on the evacuation probability of a household, i.e., as more neighbors evacuate, a household becomes more likely to evacuate. Second, concerns about property loss, via looting for example, can counteract the positive peer effect. That is, when most neighbors are away and the neighborhood is empty, the remaining households may decide not to evacuate, fearing property loss via looting. Therefore, fear of looting has a negative impact on the probability of evacuation. An important public policy goal in disaster planning and response is to increase the evacuation rates in an affected region; so understanding the interaction between these two effects becomes crucial.

1.3 Concerns over looting: motivation from other contexts

Fear of looting is an issue of importance in other related and unrelated contexts, both in the US and abroad. Concern over crime and looting was first documented in public opinion polls in the US when it ranked second in a listing of perceived national problems, in 1968 (Erskine 1974). Looting in the context of civil disturbances is discussed by Dynes and Quarantelli (1968). In fleeing the on-coming of enemies across national borders, parents may leave one of their children to guard family property, for fear of looting (Nguyen 2018). Individual looting of civilians by government soldiers is studied in Azam (2002). Financial looting has also been identified as a driver for unethical, if not illegal, profiteering by realizing financial gain with the intention of going broke later at society's expense (Akerlof et al. 1993). For these and other reasons, the study of the effects of looting on human decision-making is of interest. Here, we study it in the context of natural disasters.

1.4 Summary of results

There is a lot of work on modeling peer effects, e.g., the spread of diseases, information, fads and other contagions (Beckman et al. 2011; Chen et al. 2017; Aral and Nicolaides 2017). A number of models have been proposed, such as independent cascade (Kempe et al. 2003), and different types of threshold models, e.g., Granovetter (1978), Watts (2002), and Centola and Macy (2007). These are defined on a network, with each node in state 0 (representing non-evacuation) or 1 (representing evacuation), and a rule for a node to change state from 0 to 1. For instance, in a τ-threshold model, a node switches from state 0 to state 1 if at least a τ -fraction of its neighbors are in already in state 1. All prior models only capture the first effect above, i.e., as the number of affected neighbor increases, a node is more likely to switch to state 1. Here, we propose a new threshold model, referred to as 2MODE-THRESHOLD, which inhibits a transition from state 0 to 1 if a sufficiently large fraction of a family's neighborhood is in state 1. That is, contrary to other models, 2MODE-THRESHOLD captures the phenomenon that if too many neighbors are in state 1, then a node will not transition from 0 to 1. We demonstrate its use in a large scale study. Our results are summarized below.

1. Development of the 2MODE-THRESHOLD *model (results in Sect.* 2). We introduce and formalize evacuation decision-making as a graph dynamical system (GDS) (Mortveit and Reidys 2007; Adiga et al. 2018) using 2MODE-THRESHOLD functions at nodes. This model follows observations from surveys which show families are more likely to evacuate as more of their neighbors evacuate, but only up to a point. When too many neighbors have evacuated, a family becomes concerned about looting (crime) and hence is more likely to not evacuate (i.e., remain behind). This model is akin to threshold-characterized influence models (Granovetter 1978; Watts 2002; Schelling 2006; Centola and Macy 2007) that have been demonstrated through observations to capture decision-making, e.g., Centola (2010); Gonzalez-Bailon et al. (2011); Romero et al. (2011); Centola (2011). However, the influence only operates up to some fraction of neighbors which we denote as η_c; for fractions of neighbors $> \eta_c$, the influence to evacuate is zero.

2. Theoretical results of the 2MODE-THRESHOLD *model (results in Sect.* 3). We study the dynamics of 2MODE-THRESHOLD in different networks, and show significant differences from the standard threshold model that has no drop off.

Specifically, we find that starting at a small set of nodes in state 1, the diffusion process does not go beyond a constant fraction of the network. System configurations in which more nodes are 1's (e.g., all 1's vector of node states) are also fixed points, but our results imply that one cannot reach such fixed points with lots of 1's from most initial configurations that have a small number of 1's.

3. Social network representations of Virginia Beach, VA (results in Sect. 4). We build a family of social networks to represent Virginia Beach, Virginia, that is on the Eastern Seaboard of Virginia and was impacted by Hurricane Sandy in 2012. This region has a population of over 450,000, and households are geographically situated based on land-use data, with real geo-locations that invoke the concepts of neighbors and long range connections. Nodes in the social networks are families, and these do not change across social network instances. Rather, the edges between families, representing two forms of social influence, change. We add edges between households based on the Kleinberg small world (KSW) model (Kleinberg 1999). There are short-range and long-range directed edges, where the former is characterized by a short range distance d_{sr} in which each pair of families whose homes are with this distance are joined by an edge. The number q of long-range edges is specified, and these edges can form between two nodes at any distance $> d_{sr}$. We build networks using three values of d_{sr} and five values of q.

We characterize the networks structurally, and find the following. (1) Networks with no long-range edges never contain giant components; the largest components are about 0.35 fraction of the nodes in the entire network. (2) It is only with long-range edges that these smaller components are linked up to form giant components that encompass the entire network. The giant components appear for the least nonzero q value of 2. (3) The strongly and weakly connected components are essentially the same size and composition, even when $q > 0$. (The long-range edges are directional.) (4) The maximum in-degree of networks does *not* change as the short-range distance d_{sr} increases from 40 m to 60 m, indicating that the maximum density of homes in geographic regions do not change much when the short-range distance is changed in this range. Maximum degree increases significantly when d_{sr} increases to 100 m. Some causes of evacuation response behaviors are related to these structural properties.

4. Agent-based modeling and simulation (results in Sect. 5). We develop an agent-based model and simulation (ABMS) of the 2MODE-THRESHOLD model on realistic small world networks of Virginia Beach, VA. Our ABM enables us to capture heterogeneities in the modeling of the evacuation decision-making process. This includes not only heterogeneities in families, but also differences in (local) neighborhoods of families as represented in social networks. We use it to understand the evacuation rates in this region, and evaluate the effects of different initial conditions (e.g., number of seeds) [seeds are families who are the first ones to evacuate] on evacuation decision dynamics. A selection of results follow. (1) The variability of evacuation results (in terms of the fraction of the population that evacuates) is small across 100 seed sets. (2) The variability in evacuation rates across five network instances for a fixed pair (d_{sr}, q) is small. (3) The effects of looting—quantified by 2MODE-THRESHOLD model—can reduce evacuation rates by 50% compared to the classic Granovetter-type threshold influence model (Granovetter 1978; Watts 2002; Schelling 2006; Centola and Macy 2007). (4) The effects of network structure can be large. For example, as d_{sr} increases from 0.04 km to 0.10 km, evacuation rates can increase by 2 to 10 times. Even greater changes in the fraction of evacuating families can be observed as q increases from 0 to 16. (5) The parameters $p_{e,max}$ and η_c of the 2MODE-THRESHOLD model can produce changes in the fraction of evacuating families up to 0.38. (See Fig. 1: $p_{e,max}$ is the nonzero probability of a family evacuating.) (6) These two parameters, $p_{e,max}$ and η_c, also combine with network structure to produce interesting effects, when node degrees are large. First, as $p_{e,max}$ increases, the *rate* of increase in the *final* fraction of evacuating families can *decrease*. Second, as $p_{e,max}$ increases, the *magnitude* of the *final* fraction of evacuating families can *decrease*.

1.5 Novelty and implications

Models of type 2MODE-THRESHOLD have not been studied before. Our ABM approach can help (1) understand how planners and managers can more effectively convince

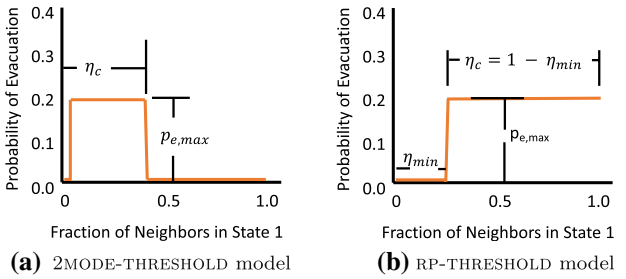

Fig. 1 Dynamics models—probability of evacuation curve—for probability p_e of evacuation for a family versus the fraction η_1 of its neighbors in state 1 (i.e., evacuating). **a** The 2MODE-THRESHOLD model: the evacuation probability is $p_e = 0$ for $\eta_1 = \eta_{min} = 0$ and for $\eta_1 > \eta_c$. The maximum probability is $p_e = p_{e,max}$ in the interval $(\eta_{min}, \eta_c]$. **b** The RP-THRESHOLD model: this curve is similar to the previous curve, except that $p_e = p_{e,max}$ for $\eta_1 > \eta_{min}$. This is a special case of 2MODE-THRESHOLD, but is a variation of the regular probabilistic threshold model (Watts 2002; Centola and Macy 2007). As an illustration, if an agent has 50% of its neighbors in state 1, then the model in **a** shows that $p_e = 0$, while **b** shows that $p_e = p_{e,max} > 0$. An example with values for these parameters is given in the text

families that are in harms way to evacuate; (2) understand the effects of families' social networks on evacuation decisions (Widener et al. 2013; Ferris et al. 2016; Yang et al. 2019); and (3) establish downstream conditions after the evacuation decision has been made, to support additional types of analyses. For example, the results from these studies can be used to forecast traffic congestion (spatially and temporally) during the exodus (Madireddy et al. 2015), and to determine places where shelters and triage centers should be established. We put our work in the context of previous works in Related Work, Sect. 6.

1.6 Extensions from preliminary version

A preliminary version of this paper appears in (Halim et al. 2020). The contents of that paper are extended in the following ways. (1) The number of types of networks (characterized by (d_{sr}, q) pairs) is 3× that in the preliminary version. (2) Structural properties of these Virginia Beach, VA networks are presented and contrasted. (3) Many more simulation parameters have been considered and analyzed. (4) A more thorough analysis of the parameter values is done. Accordingly, the number of simulations has increased by over 300%, and the number of results shown in plots has increased threefold.

1.7 Paper organization

The graph dynamical systems (GDS) framework and the 2MODE-THRESHOLD model are presented in Sect. 2. Theoretical results are provided in Sect. 3. Social network construction and networks are described and characterized in Sect. 4. Section 5 describes the simulation process and presents simulation results. Section 6 provides related work, and conclusions are in Sect. 7.

2 Evacuation decision-making model

2.1 Motivation from social science

Our model is motivated by the analysis of a survey in the counties affected by Hurricane Sandy in the northeastern USA by Halim and Mozumder (2020) which is briefly summarized here. The goal of this survey was to assess factors driving evacuation decisions (Meng and Mozumder 2020). The survey had a response rate of 61.93%, with over 1200 responses. A Binomial Logit model was applied to the survey data and tested for the factors associated with households' evacuation behaviors (Halim and Mozumder 2020). The results indicate that a respondent's employment status, consideration of neighbors' evacuation behavior, concerns about neighborhood criminal activities or looting, access to the internet in the household, age, and having flood insurance, each plays a significant role in a respondent's decision to evacuate during Hurricane Sandy. Noteworthy was the influence of neighbors' evacuation behaviors, and concerns about looting and criminal behavior. Neighbors' evacuations had a statistically significant and positive effect on evacuation probability but concerns about criminal and looting behavior had a significant negative effect—implying that if too many neighbors left, then the remaining households are less likely to evacuate.

2.2 A graph dynamical systems framework

A *graph dynamical system* (GDS) (Mortveit and Reidys 2007; Adiga et al. 2018) is a mathematical abstraction that is used to build quantitative models of human behavior. These models can be used in agent-based modeling (ABM) approaches. We use it here to develop a model of evacuation behavior, motivated by the survey analysis described above. A GDS $\mathcal{S}$ describes the evolution of the states of a set of agents. Let $\mathbf{x^t} \in \{0,1\}^n$ denote the vector of agent states at time t, with $x_v^t = 1$ indicating that agent v has evacuated. $x_v^t = 0$ means that agent v has not evacuated at time t. A GDS $\mathcal{S}$ consists of two components: (1) an interaction network $G = (V, E)$, where V represents the set of agents (in our case, the households which are deciding whether or not to evacuate), and E represents a set of edges, with $e = \{u, v\} \in E$ if agents u and v can influence each other; and (2) a set $\mathcal{F} = \{f_v : v \in V\}$ of *local* functions $f_v : \{0,1\}^{deg(v)} \to \{0,1\}$ for each node $v \in V$, which determines the state of node v in terms of the states of $N(v)$, the set of neighbors of v. Given a vector $\mathbf{x^t}$ describing the states of all agents at time t, the vector $\mathbf{x^{t+1}}$ at the next time is obtained by updating x_v^{t+1} using its local function $f_v(\cdot)$. We say that a state vector $\mathbf{x^t}$ is a *fixed point* of $\mathcal{S}$ if the node states do not change, i.e., $\mathbf{x^{t+1}} = \mathbf{x^t}$.

2.2.1 The 2MODE-THRESHOLD local functions: modeling evacuation behavior

The 2MODE-THRESHOLD function $f_v(\cdot)$ will be probabilistic, and will depend on the *probability of evacuation*, in order to capture the qualitative aspects of the results of Halim and Mozumder (2020). This is shown in Fig. 1a and specifies the probability of evacuation p_e for agent v_i as a function of the fraction η_1 of neighbors of v_i in state 1. We have $p_e = p_{e,max}$ for $\eta_1 \in (\eta_{min}, \eta_c]$, and $p_e = 0$ for $\eta_1 \in [0, \eta_{min}]$ and $\eta_1 > \eta_c$. In this paper, we primarily focus on $\eta_{min} = 0$. Specifically, this captures the following effects: (1) peer (neighbor) influence can cause families to evacuate and (2) if too many of a family's neighbors evacuate, there are not enough neighbors remaining behind to dissuade potential looters, so a family reduces its probability of evacuation. The first effect makes $p_e = p_{e,max}$ for $\eta_1 > 0$, and the second effect results

in p_e dropping to zero at $\eta_1 = \eta_c$. Note that the special case where $p_e = p_{e,max}$ for $\eta_1 > \eta_{min} = 0$ is a probabilistic variant of the η_{min}-threshold function (e.g., Centola and Macy 2007); we will sometimes refer to this as the "regular probabilistic threshold" model, and denote it by RP-THRESHOLD. This model is shown in Fig. 1b. These are models that can be assigned to any agent; in GDS, an agent is a node that resides in a networked population.

2.2.2 Network models

We present the details of the network construction process in Sect. 4.1. We summarize the notation of a social network here. The contact network $G = (V, E)$ is the other component of a GDS $\mathcal{S}$. A node $v_i \in V$, represents a family, or a household. Edges represent interaction channels, for communication and observations. Edges are *directed*: a directed edge $(v_j, v_i) \in E$, with $v_i, v_j \in V$, means that family v_j *influences* family v_i.

2.3 Example of GDS

Figure 1a shows an example of the 2MODE-THRESHOLD model with the parameters $p_{e,max} = 0.2$, and $\eta_c = 0.4$. Figure 1b shows a RP-THRESHOLD model. The purpose of this example is to illustrate the dynamics of these models on a network of five agents. In Fig. 2, $\mathbf{x^0}$ is the initial configuration with node 1 evacuated (in state 1, shaded), and nodes 2, 3, 4, and 5 not evacuated (in state 0, not shaded). Nodes 2 and 3 have $\eta_1 = 1/3 < \eta_c = 0.4$, and so for both of them, the evacuation probability is $p_e = 0.2$. Nodes 4 and 5 have $\eta_1 = 0$, so $p_e = 0$ for them. Therefore, the probability that the state vector is $\mathbf{x^1}$ at the next time step (see Fig. 2) is $p_{e,max}(1 - p_{e,max}) = 0.2 \cdot 0.8 = 0.16$, since only node 2 switches to 1. With respect to the configuration $\mathbf{x^1}$, nodes 3, 4, and 5 have $\eta_1 = \frac{2}{3}$, 1 and 0, respectively. Therefore, $p_e = 0$ for all these nodes, and $\mathbf{x^1}$ is a fixed point of the $\mathcal{S}$ with the 2MODE-THRESHOLD functions. However, for the regular probabilistic threshold model, RP-THRESHOLD, with $\eta_{min} < 0.3$, $\mathbf{x^1}$ is not a fixed point, since nodes 3 and 4 both have $p_e = p_{e,max}$ probability of transitioning (since they have $\eta_1 > \eta_{min}$). Therefore, in the regular probabilistic threshold model, RP-THRESHOLD, $\mathbf{x^1} \to \mathbf{x^2}$ transition occurs with probability $p^2_{e,max} = 0.04$.

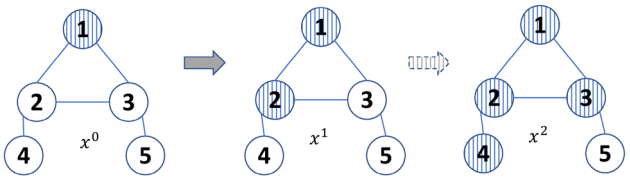

Fig. 2 An example showing the transitions in a $\mathcal{S}$ on a graph with five nodes, and 2MODE-THRESHOLD local functions, with parameters $p_{e,max} = 0.2$ and $\eta_c = 0.4$. The figure shows a transition of the dynamics model from configuration $\mathbf{x^0}$ to $\mathbf{x^1}$, with shaded nodes indicating evacuation. The $\mathbf{x^0} \to \mathbf{x^1}$ transition occurs with probability $p_{e,max}(1 - p_{e,max}) = 0.16$. For the above parameters, $\mathbf{x^1}$ is a fixed point, and the node states do not change. However, if we had $\eta_c = 1$ (i.e., this is a regular probabilistic threshold), $\mathbf{x^1}$ is not a fixed point, and there can be a transition to configuration $\mathbf{x^2}$ with probability $p^2_{e,max} = 0.04$ (indicated as a dashed arrow)

2.4 Problems of interest

We will refer to a GDS system $\mathcal{S}_{2m} = (G, \mathcal{F})$ in which the local functions are 2MODE-THRESHOLD functions as a 2MODE-THRESHOLD-GDS. Our objective in this paper is to study the following problems on a $\mathcal{S}_{2m}$ system:

(1) How do the dynamical properties of 2MODE-THRESHOLD GDS systems differ from those of $\mathcal{S}$ with RP-THRESHOLD model functions? Do they have fixed points, and what are their characteristics?
(2) How do the number of 1's in the fixed point depend on the initial conditions, and the model parameters, namely $p_{e,max}$ and η_c? How can this be maximized?

We provide solutions to these problems next.

3 Analyzing dynamical properties in different network models

It can be shown that any $\mathcal{S}_{2m}$ converges to a fixed point in at most $n/p_{e,max}$ steps. $\mathcal{S}_{2m}$ systems have significantly lesser levels of diffusion (i.e., number of nodes ending up in state 1), compared to the RP-THRESHOLD model, as we discuss below.

Lemma 1 *Consider a $\mathcal{S}_{2m}$ with $G = K_n$ being a complete graph on n nodes. Starting at a configuration $\mathbf{x^0}$ with a single node in state 1, $\mathcal{S}_{2m}$ converges to a fixed point with at most $(p_{e,max} + \eta_c)n$ nodes in state 1, in expectation. In contrast, in a regular probabilistic threshold system on K_n with $\eta_{min} = 0$, the system converges to the all 1's vector $\mathbf{x^t}$ as a fixed point.*

Proof Consider the 2MODE-THRESHOLD model and a state vector $\mathbf{x^t}$ with k nodes in state 1. Consider any node v with $\mathbf{x^t}_v = 0$. If $k \le \eta_c n$, then, Pr[node v switches to 1] $= p_{e,max}$. Therefore, the expected number of nodes which switch to 1 is $p_{e,max}(n - k) \le np_{e,max}$. If $k > \eta_c n$, for every node in state 0, the probability of switching to 1 is $p_e = 0$. Therefore, the expected number of 1's in a fixed point is at most $np_{e,max} + n\eta_c$. On the other hand, in a regular probabilistic threshold model RP-THRESHOLD, the system does not converge

until each node in state 0 switches to 1 (since $p_e = p_{e,max}$ for all $\eta_1 > 0$). □

We observe below that starting at an initial configuration with a single node in state 1, $\mathcal{S}_{2m}$ converges to a fixed point with at most a constant fraction of nodes in state 1. Note, however, that configurations $\mathbf{x}^t$ with more than that many nodes in state 1, e.g., the all 1's vector, are also fixed points. The result below implies that those fixed points will not be reached from an initial configuration with a few 1's.

Lemma 2 *Consider a $\mathcal{S}_{2m}$ on a $G(n, p)$ graph with $p\eta_c \geq \frac{6}{\epsilon^2}\frac{\log n}{n}$, for any $\epsilon \in (0, 1)$. Starting at a configuration $\mathbf{x}^0$ with a single node in state 1, $\mathcal{S}_{2m}$ converges to a fixed point with at most $(1 + 2\epsilon)(\eta_c + p_{e,max})n$ nodes in state 1, in expectation. In contrast, in a regular probabilistic threshold system on K_n with $\eta_{min} = 0$, the system converges to the all 1's vector as a fixed point.*

Proof (Sketch) Let $deg(v)$ denote the degree of v. For a subset S, let $deg_S(v)$ denote the degree of v with respect to S, i.e., the number of neighbors of v in S. For any node v, we have $E[deg(v)] = np$. By the Chernoff bound (Dubhashi and Panconesi 2009), it follows that $\Pr[deg(v) > (1 + \epsilon)np] \leq e^{-\epsilon^2 np/3} \leq 1/n^2$. Consider a set S of size $\frac{1+\epsilon}{1-\epsilon}\eta_c n$. For $v \notin S$, $E[deg_S(v)] = |S|p$, and so $\Pr[deg_S(v) < (1 - \epsilon)|S|p] \leq e^{-\epsilon^2|S|p/2} \leq 1/n^2$. For $|S| \geq \frac{1+\epsilon}{1-\epsilon}\eta_c n$, we have $(1 - \epsilon)|S|p \geq (1 + \epsilon)\eta_c np$. Putting these together, with probability at least $1 - 2/n$, we have $deg(v) \leq (1 + \epsilon)np$ and $deg_S(v) \geq (1 + \epsilon)\eta_c np \geq \eta_c deg(v)$, for all nodes v. Therefore, if $\mathcal{S}_{2m}$ reaches a configuration with nodes in set S of size $\frac{1+\epsilon}{1-\epsilon}\eta_c n < (1 + 2\epsilon)\eta_c n$, with probability $1 - 2/n$, S is a fixed point. With probability $\leq 2/n$, S is not a fixed point, and the process converges to a fixed point with at most n 1's, so that the expected number of 1's in the fixed point is at most $|S| + 2 \leq (1 + 2\epsilon)\eta_c n$. On the other hand, consider the last configuration S' which has size $|S'| < (1 + 2\epsilon)\eta_c n$. Then, in expectation, at most $p_{e,max}n$ additional nodes switch to state 1, after which point, the configuration has more than $(1 + \epsilon)\eta_c n$ 1's. Therefore, the expected number of 1's in the fixed point is at most $(1 + 2\epsilon)(\eta_c + p_{e,max})n$. □

4 Social networks

4.1 Network construction and semantics

We describe the models for the contact network $G = (V, E)$, which is another component of a GDS $\mathcal{S}$. A node $v_i \in V$ represents a family, or a household. Edges represent interaction channels, for communication and observations. Edges are *directed*: a directed edge $(v_j, v_i) \in E$, with $v_i, v_j \in V$, means that family v_j *influences* family v_i. We use the synthetic population model developed in Barrett et al. (2009) for representing the set V of households.

The synthetic population of Virginia Beach VA, is a set of individuals each endowed with demographic variables drawn from the US census. Each synthetic individual is placed in a household with other individuals and each household is located geographically in such a way that if it is aggregated to a block group level, a census of this synthetic population will yield results that are statistically indistinguishable from the original census data.

In particular, the locations of all households (family residences) are determined, which result in longitude, latitude (i.e., lon, lat) coordinates for each household. These are used to compute distances between family residences.

Figure 3 summarizes the process of producing a social network on the families of a city. Edges are specified using the Kleinberg small world (KSW) network approach (Kleinberg 1999), and there are two types of edges: short range and long range. Short-range edges (v_j, v_i) represent either (1) a family v_i speaks with (is influenced by) another family v_j in the neighborhood about evacuation decisions, or (2) a family v_i observes v_j's home and infers whether or not a family v_j has evacuated. A long-range edge represents a member of one family v_i interacting with another family far away who is a relative or friend or colleague at work v_j. Each edge has a label of distance between homes, using (lon, lat) coordinates of each home. Thus, the KSW model has the following parameters: the node set V and their attributes, the short-range distance d_{sr} over which short-range edges are placed

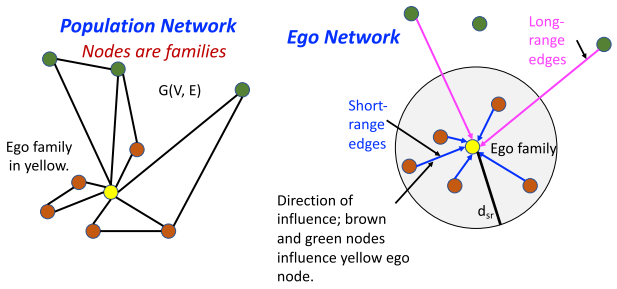

Fig. 3 (Left) Depiction of a toy population network with families represented as nodes and edges representing possible interactions. (Right) Focus on the yellow ego node and the edges for families that influence it. The nodes are the same as those on the left plot. Ego node (in yellow) and edges formed using the KSW process. Short-range edges (blue) are formed with the ego family by identifying all families (brown) within short-range distance d_{sr} of the ego family. A number q of long-range edges (magenta) are selected at random from all families (green) located at distance greater than d_{sr} from the ego family. (In this figure, $q = 2$.) All edges are directed to the ego family, i.e., all brown and green nodes with edges to the ego node influence the ego node. All (lon,lat) coordinate locations are for family households (Color figure online)

between nodes, and the number q of long range edges incident on each node v_i. For each node v_i, (1) short-range edges (v_j, v_i) are constructed, where $d(v_j, v_i) \leq d_{\text{sr}}$; and (2) q long-range edges (v_k, v_i) are placed at random, with probability proportional to $1/d(v_k, v_i)^{\alpha}$, for a parameter α. Note that for each short-range edge (v_j, v_i), there is a corresponding edge (v_i, v_j). See Kleinberg (1999) for details. Semantics of edges, for our application, are provided in Fig. 4.

4.2 Networks

Table 1 provides the social networks (and selected properties) that are used in simulations of evacuation decision making. The network model of Sect. 4.1 was used to generate KSW networks for Virginia Beach, VA. Inputs for the model were $n = 113967$ families forming the node set V, with (lat, long) coordinates; $d_{\text{sr}} = 40$, 60, and 100 m; $\alpha = 2.5$ (see Kleinberg 1999); and $q = 0$ to 16. Five graph instances were generated for each (d_{sr}, q) combination. Network properties are discussed in the next subsection.

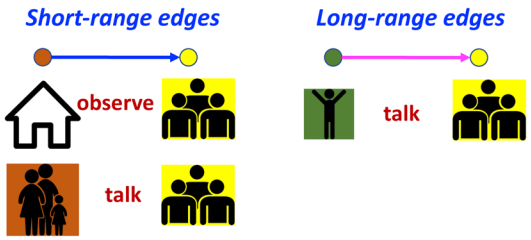

Fig. 4 Semantics of edges into yellow ego node, from Fig. 3. (Left) Short-range edges can mean that the ego family observes neighboring families' evacuation statuses, or talks to neighbors. (Right) Long-range edges represent friends, relatives, or coworkers who live far away from the ego family

4.3 Structural properties

Structural analyses were performed with SNAP (Leskovec and Sosič 2016) and NetworkX (Hagberg et al. 2008) through the codes in the *net.science* cyberinfrastructure (Ahmed et al. 2020).

4.3.1 Number of graph edges as a function of d_{sr} and q

Figure 5 shows the number of edges in graphs, as a function of graph structure. This structure is given by the short-range distance d_{sr} and the deterministic edges that result, and the number q of stochastic long-range edges. (Stochasticity comes in the from of what nodes v_k form q long-ranges edges (v_k, v_i) with node v_i.) From the graph generation description above the number of edges will be linear in q, as shown. The data at $q = 0$ shows the effect of d_{sr}; a nonlinear effect of d_{sr} on the number of edges.

4.3.2 In-degree and out-degree distributions

Figure 6 shows the in-degree distributions for the different classes of networks. The plots, left to right, are for d_{sr} values

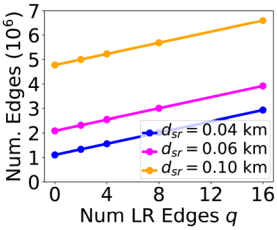

Fig. 5 Count of edges in each type class of network, where each class is given by the pair (d_{sr}, q). Number of edges is in millions

Table 1 Kleinberg small world (KSW) networks used in our experiments and their properties

Network class	Distance for short-range edges, (m)	Num LR edges	Avg. in-deg. (= avg. out-deg.)	Max. in-deg.	Max. out-deg.
KSW0	40, 60, 100	0	10.11, 18.56, 41.98	380, 380, 432	380, 380, 432
KSW2	40, 60, 100	2	11.70, 20.34, 43.86	382, 382, 434	381, 383, 438
KSW4	40, 60, 100	4	13.70, 22.34, 45.86	384, 384, 436	381, 383, 445
KSW8	40, 60, 100	8	17.70, 26.34, 49.86	388, 388, 440	382, 383, 449
KSW16	40, 60, 100	16	25.70, 34.34, 57.86	396, 396, 448	383, 384, 469

The number n of nodes is 113,967 for all graphs. The short-range distance d_{sr}, over which short-range edges are constructed with probability of 1.0, ranges from 40 meters to 100 meters. The exponent $\alpha = 2.5$ is for computing the probabilities of selecting nodes with which to form long-range edges with each node $v_i \in V$. Column "Num LR Edges", i.e., (q) means number of long-range edges incoming to each node v_i; the edges are chosen randomly. There are five graph instances for every (d_{sr}, q) combination. Average degree is d_{ave} and maximum degree is d_{max}, for in-degree and out-degree. There are three values for each degree heading, one corresponding to each of the three values of d_{sr} in the second column. For example, for KSW2 (where $q = 2$), and $d_{\text{sr}} = 40$, 60, and 100 m, the average degrees in the graphs are, respectively, 11.70, 20.34, and 43.86

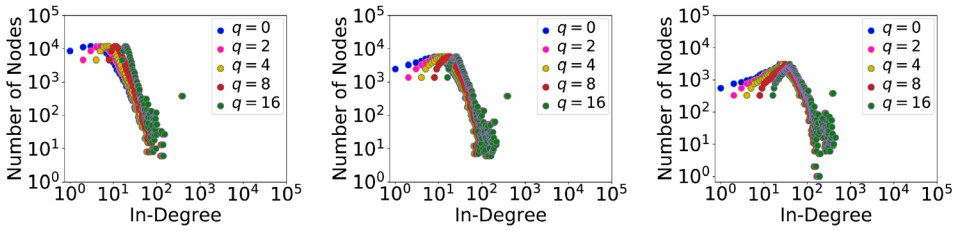

(a) $d_{sr} = 0.04$ km, all q **(b)** $d_{sr} = 0.06$ km, all q **(c)** $d_{sr} = 0.1$ km, all q

Fig. 6 In-degree distributions for the classes of networks. Distributions for all (d_{sr}, q) combinations are provided. **a** $d_{sr} = 0.04$ km networks, instance 0. **b** $d_{sr} = 0.06$ km networks, instance 0. **c** $d_{sr} = 0.10$ km networks, instance 0. The degree distributions for the other instances are very close to these; for the case $q = 0$, the degree distributions are identical because these graphs have determinstically-placed edges. The same 113,967 nodes, representing families, comprise the node set of each graph

of 0.04 km, 0.06 km, and 0.10 km. In each plot are degree distributions for q values of 0 through 16, in powers of 2. Figure 7 shows the respective out-degree distributions for the different classes of networks.

Essentially, in-degree distributions, per (d_{sr}, q), take the same form, but shift to the right in Fig. 6 because as q increases, the in-degree of each node v_i increases: q is the number of long-range edges added per v_i (the directed edge is oriented *in* to v_i), to the graph of short-range edges. The out-degree distributions in Fig. 7 also shift to the right as q increases in each plot, but there are now small numbers of nodes with small degrees because tail nodes are selected randomly for each head node, for long-range edges. (A directed edge (v_j, v_i) is the edge from v_j to v_i, where v_j is the tail node and v_i is the head node.)

It is interesting that the maximum in-degrees for $d_{sr} = 40$ m are the same as those for $d_{sr} = 60$ m in Table 1. This is due to the "isolation" of a dense region that does not reach other nodes as d_{sr} increases in this range. (The average degree does increase for $d_{sr} = 60$ m, and one can see this increase in the entire degree distribution, except for the maximum degree. For example, the number of nodes with the maximum degree increases.) However, when d_{sr} increases further to 100 m, the maximum in-degree increases substantially.

The average in-degree and out-degree values are in the fourth column of Table 1 for, respectively, $d_{sr} = 0.04$, 0.06, and 0.1 km. The set of three values in successive rows are for increasing q values (Num LR Edges). Note that these average degrees increase by the increase in q in going from one row to the next, except for the case in going from $q = 0$ to $q = 2$. When $q = 0$, some nodes are isolated and therefore are not considered in the structural properties. When $q > 0$, all nodes form edges because of the way long-range edges are constructed.

4.3.3 Strongly and weakly connected components in graphs

Graphs are broken into two groups, depending on their sizes of weakly connected components (WCCs). The first group is those networks where $q = 0$ for all d_{sr} values: these graphs do not form a single component, or even a giant component. The largest component is 0.35 fraction of nodes for $d_{sr} = 0.10$ km (defining a giant component to be at least one-half of nodes). The second group of networks is $q \geq 2$ for all d_{sr}, where all nodes (or for $d_{sr} = 0.04$ km, almost all nodes) are in one component. See Table 2.

As the Table 2 caption indicates, the strongly connected components (SCCs) are of comparable sizes to the WCC

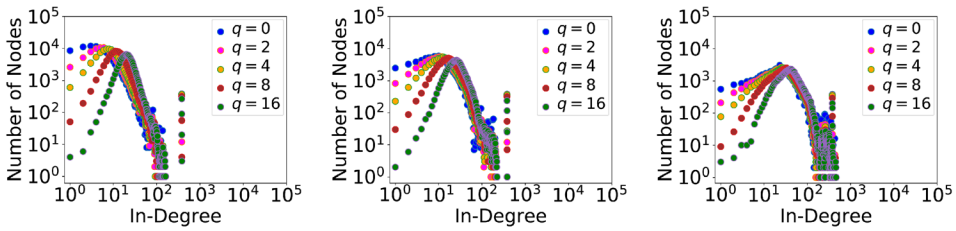

(a) $d_{sr} = 0.04$ km, all q **(b)** $d_{sr} = 0.06$ km, all q **(c)** $d_{sr} = 0.1$ km, all q

Fig. 7 Out-degree distributions for the classes of networks. Distributions for all (d_{sr}, q) combinations are provided. **a** $d_{sr} = 0.04$ km networks, instance 0. **b** $d_{sr} = 0.06$ km networks, instance 0. **c** $d_{sr} = 0.10$ km networks, instance 0. The degree distributions for the other instances are very close to these; for the case $q = 0$, the degree distributions are identical because these graphs have deterministically-placed edges. The 113,967 families, comprise the node set of each graph

Table 2 Sizes of weakly connected components (WCCs) and strongly connected components (SCCs) for the Kleinberg small world (KSW) networks

d_{sr} (km)	q	Size (fraction of nodes) of Largest connected component
0.04	0	381 (0.0035)
0.04	$q = 2$	113,955 (> 0.99)
0.04	$q \geq 4$	113,967 (1.0)
0.06	0	6146 (0.055)
0.06	$q \geq 2$	113,967 (1.0)
0.10	0	39,287 (0.35)
0.10	$q \geq 2$	113,967 (1.0)

The table values are for the WCCs. The largest SCCS are of approximately the same size; the differences, if any, are on the order of 1% to 2% at most

sizes. The component sizes for $q = 0$ are identical to the WCC sizes because the short-range edges are bidirectional. For $q \geq 2$, the SCC sizes are within a percent or two of the WCC sizes.

Hence, the long-range edges are accomplishing what they are designed to do in the Kleinberg network generation process: they provide non-local edges, that in these cases, connect otherwise disparate components. This is important because these longer-range edges enable the evacuation contagion, in the simulations in Sect. 5, to spread throughout the graphs.

5 Agent-based simulations and results

5.1 Simulation process

Inputs to a simulation are a social network (Sect. 4), a set of local functions that quantifies the evacuation decision making process of each node $v_i \in V$ (see Sect. 2), and a set of *seed* nodes whose state is 1 (i.e., these nodes are set to "evacuate" at the start of a simulation at time $t = 0$). All other nodes at time $t = 0$ are in state 0 (the non-evacuating state). We vary a number of input parameters across simulations. Each *simulation instance* or *run* consists of a particular set of seed nodes at $t = 0$, and time is incremented in discrete timesteps, from $t = 0$ to t_{max}. Here, $t_{max} = 10$ days, to model the ten days *leading up to* hurricane arrival. Hurricane arrival is day 10. At each timestep, nodes that are in state 0 may change to state 1, per the models in Sect. 2. At each $1 \leq t \leq t_{max}$, the state of the system at time $t - 1$ is used to compute the next state of each $v_i \in V$ (corresponding to time t) *synchronously*; that is, all nodes (families) v_i update their states in parallel at each t. A simulation consists of 100 runs, where each run has a different seed set. The network and dynamics model are fixed in a simulation across runs.

Since each social network has the same node IDs (that represent families), we use the same seed collection for a specified number n_s of seed nodes. Since there are 100 runs per simulation, there are 100 seed sets within one seed collection. Thus, as an example, a simulation with a graph such that $d_{sr} = 0.06$ km and $q = 4$ uses the same 100 seeds sets as a simulation on a graph with $d_{sr} = 0.1$ km and $q = 16$, for a specified value of n_s. This eliminates variability in seed sets when assessing effects of graph structure.

The results below are plotted in groups of simulations. That is, each plot typically contains results for many simulations. The results from the 100 runs of a simulation are typically averaged, and error bars on results (indicating one standard deviation) are also commonly provided.

5.2 Simulation parameters studied

The input parameters varied across simulations are provided in Table 3. The results in subsequent subsections investigate the effects of these variables on the (population-level) fraction of families that evacuate, designated by "Frac. Evac." We study and present results for all of the parameter values.

5.3 Simulation results

We note that in the results that follow, the y-axis value ranges can change across figures. This is because the 2MODE-THRESHOLD model and the RP-THRESHOLD model can give widely different results, and depending upon the parameter values, the results can vary greatly with-in a model too. Therefore, y-axis ranges are one of 0 to 0.1, 0 to 0.4, or 0 to 1.0.

The results are broken down by types of results in Table 4. Subsections of this manuscript containing the results are given. First, fraction of families that evacuate owing to a simple uniform mixing model are given, to contrast with the ABS results in all other subsections. The basic ABS results are then given, showing time histories of how the fraction of evacuating families increases with time. Next, since our social networks are particular instances of *families* of networks, for a fixed d_{sr} and q, the effects of the graph structure of particular graph instances, for fixed d_{sr} and q, on evacuation predictions are given. The next subsection contrasts the looting model of this work, the 2MODE-THRESHOLD model, with the more classic contagion model, referred to herein as the RP-THRESHOLD model, that does not consider looting effects. All subsequent subsections of the results focus on the 2MODE-THRESHOLD model, and we study, in turn, the effects of network structure (as specified by d_{sr} and q), of model parameters (through $p_{e,max}$ and η_c), and of initial conditions.

Table 3 Description of the parameters and their values used in the simulations

Parameter	Description
Networks d_{sr}, q	Networks in Table 1. We vary the number q of long-range incoming edges per node, per the table, from 0 to 16. The short-range distance d_{sr} takes values 0.04 km, 0.06 km, and 0.10 km
Network instances	There are five network instances for each network, labeled 0 to 4
Num. random seeds, n_s	Number of seed nodes specified per run (chosen uniformly at random). Values are 50, 100, 200, 300, 400, and 500
Threshold model	The 2MODE-THRESHOLD model of Fig. 1a and the RP-THRESHOLD (i.e., classic) threshold model of Fig. 1b, in Sect. 2
Threshold range, η_c	The range in relative degree over which nodes can change to state 1. Discrete values are 0.1, 0.2, 0.4, 0.5, 0.6, 0.8, and 1.0. Note that $\eta_c = 1$ corresponds to the classic stochastic threshold RP-THRESHOLD model (Fig. 1b), whereas values of $\eta_c < 1$ correspond to the 2MODE-THRESHOLD model (Fig. 1a)
Maximum probability, $p_{e,max}$.	The maximum *daily* probability of evacuation $p_{e,max}$ of Fig. 1. Discrete values are 0.01 to 0.07 in 0.01 increments; 0.10, 0.15, 0.20, and 0.25.
Simulation duration t_{max}.	The duration of all simulations is the 10 days leading up to hurricane impact. Day 10 is hurricane impact.
Num. of simulation runs	100 runs per each combination of variables, where, given a particular number n_s of seed nodes, there are 100 different sets of seed nodes, all of size n_s. This collection of 100 seed sets is the same for all runs where this n_s is specified. For example, it is the same for the two cases: $(d_{sr}, q) = (0.04\ \text{km}, 4)$ and $(d_{sr}, q) = (0.1\ \text{km}, 16)$, when the specified number of seed nodes is n_s.

Table 4 Results are grouped into the following subsections

Section of results	Type of results	Description
5.3.1	Uniform mixing results	Simple results for contagion spreading of evacuation for a uniform mixing population, to contrast with the ABS results
5.3.2	Basic results	Curves showing basic trends in the dynamics of families evacuating
5.3.3	Network variability	The results showing that computed spread fractions do not vary significantly across graph instances for a *fixed* d_{sr} and q
5.3.4	Model differences	Highlight fundamental differences between the 2MODE-THRESHOLD model and the RP-THRESHOLD model of Fig. 1. Also studies the transition between these two models with η_c
5.3.5	Network structure	The results showing that computed spread fractions vary significantly for *varying* d_{sr} and q
5.3.6	Model parameters	Shows the effects of model parameter values for $p_{e,max}$ in the 2MODE-THRESHOLD model
5.3.7	Model parameters plus network structure	Shows counter-intuitive effects in evacuation rates. Increases in $p_{e,max}$ can lower evacuation rates in the 2MODE-THRESHOLD model
5.3.8	Initial conditions	Shows the effects of number of seed nodes n_s in the 2MODE-THRESHOLD model

5.3.1 Results of a uniformly mixing population

Daily evacuation probability values for a family—$p_{e,max}$ in Table 3—for both the 2MODE-THRESHOLD model (Fig. 1a) and the RP-THRESHOLD model (Fig. 1b), are converted to evacuation probability at any time over a ten-day period in Table 5. The fraction of a population that evacuates in the face of a hurricane can reach 50% or more (Hasan and Ukkusuri 2011; Widener et al. 2013; Yang et al. 2019). The values in this table do not account for evacuation-dampening effects like the fear of looting addressed in this work. Doing so, as we will see in the results below, produces population-level evacuation fractions below 50%, and often less than 1/2 of the evacuation rates of the RP-THRESHOLD model. Hence, we examine individual probability values $p_{e,max}$ of greater value, and because of the 2MODE-THRESHOLD model, evacuation rates are not excessive.

Table 5 Family-level probability of evacuation at any time over the ten days prior to hurricane landfall, as a function of family-based daily probability of evacuation, according to $p_{10days} = 1 - (1 - p_{daily})^{t_{max}}$

Daily probability $p_{daily} = p_{e,max}$	**Probability of evacuation any time over 10 days**
0.01	0.0956
0.02	0.183
0.03	0.263
0.04	0.335
0.05	0.401
0.06	0.461
0.07	0.516
0.08	0.566
0.09	0.611
0.10	0.651

5.3.2 Basic agent-based simulation results

Figure 8 provides average fraction of evacuating families (Frac. Evac.) as a function of time in days. Time moves left to right in each plot, starting ten days before hurricane landfall and ending with hurricane landfall on the tenth day (day 10). The two plots in the upper row are fractions of families deciding to evacuate on the specified day, i.e., these are instantaneous fractions of *new* evacuating families. The two plots in the lower row are the corresponding plots for the *cumulative* fraction of families evacuating. We use the 2MODE-THRESHOLD model with $p_{\text{e,max}} = 0.15$ and $\eta_{\text{c}} = 0.2$ (see Fig. 1a). The two plots in the left column differ from those in the right column in the number q of long-range edges in the graphs: on the left, there are $q = 4$ long-range incoming edges per node and on the right, there are $q = 16$ long-range incoming edges per node. Each plot contains six curves, for different numbers of seed nodes (nodes [families] deciding to evacuate at time $t = 0$), ranging from 50 to 500. As number n_s of random seeds increases, the curves shift left for the fractions of new families evacuating, in the top row of plots, meaning that more families are evacuating earlier. Accordingly, in the bottom row of plots, at each day, the cumulative fractions f_{de} of families evacuating increases as n_{s} increases. Also, the fractions of evacuating families increases as the number q of long-range edges increases.

Error bars indicate one standard deviation in results across 100 runs (i.e., simulation instances). The standard deviation is very small (the bars are difficult to see in the plots). Based on the very small variances in these and other plots, we say no more about the variance in outputs across the 100 runs comprising a simulation. Also, because we are interested in the cumulative fraction of families evacuating, we will focus on these plots, rather than the fraction of instantaneously (or newly) evacuating families.

5.3.3 Variability of results across graph instances

Figure 9 provides a series of plots that show the final fraction of families evacuating (Final Frac. Evac.) for five graph instances (different graph instances) in each plot. The goal is to determine the variability in computed evacuation fractions across graph instances for the same nominal graph construction values. Specifically, as described in Sect. 4, a graph instance is specified by the short-range distance d_{sr} and the number q of long-range incoming edges per node.

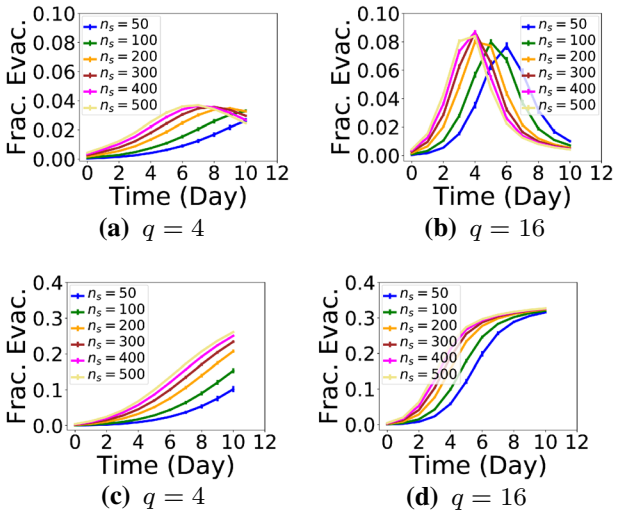

(a) $q = 4$ **(b)** $q = 16$ **(c)** $q = 4$ **(d)** $q = 16$

Fig. 8 Simulation results of the fraction of families deciding to evacuate (Frac. Evac.) as a function of time leading up to the hurricane arrival. We are always modeling the 10 days leading up to the arrival of a hurricane. Day 10 is the arrival of the hurricane; time zero is the start of the simulation—ten days prior to hurricane landfall. The network here is instance 0 of the **a** and **c** KSW4 network class ($q = 4$) and $d_{\text{sr}} = 40$ m, and **b** and **d** KSW16 network class ($q = 16$) and $d_{\text{sr}} = 40$ m. The model is 2MODE-THRESHOLDwith $p_{\text{e,max}} = 0.15$. The two plots in the top row are the fractions of newly evacuating families at each day. The two plots in the bottom row are the cumulative fractions of evacuating families up to, and including, that day. The two plots in the top row have different y-axis ranges than the plots in the bottom row. Error bars denoting one standard deviation from the means are plotted each integer unit time, but are very small

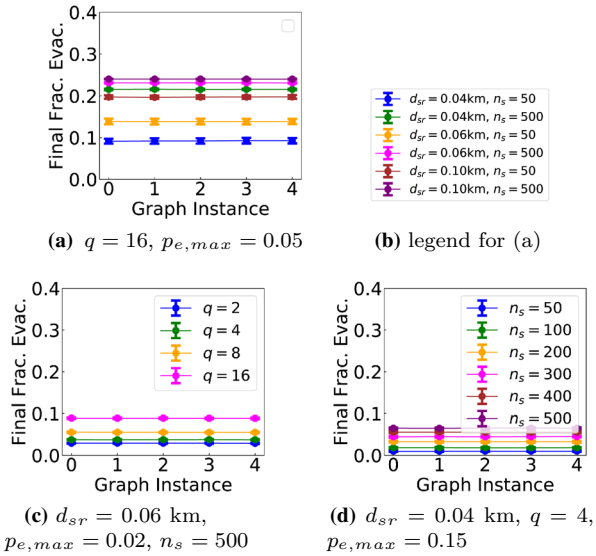

(a) $q = 16$, $p_{e,max} = 0.05$ **(b)** legend for (a) **(c)** $d_{sr} = 0.06$ km, $p_{e,max} = 0.02$, $n_s = 500$ **(d)** $d_{sr} = 0.04$ km, $q = 4$, $p_{e,max} = 0.15$

Fig. 9 Simulation results of the fraction of families deciding to evacuate (Frac. Evac.) as a function of graph instance. These plots present variability in results across particular graph instances (0 through 4 on x-axis), for the same graph generation parameters. **a** all d_{sr} values, $q = 16$, $p_{\text{e,max}} = 0.05$, and $n_{\text{s}} = 50$ and 500. **c** legend for the plots in **b**. **d** $d_{\text{sr}} = 0.06$ km, all q values, $p_{\text{e,max}} = 0.02$, and $n_{\text{s}} = 500$. **e** $d_{\text{sr}} = 0.04$ km, $q = 4$, $p_{\text{e,max}} = 0.15$, and all n_{s} values. Emphasis is on conditions that do *not* reach the looting-induced spread fraction ceiling, as in Fig. 8d, since this will drive down variability. Error bars denoting one standard deviation from the means are plotted each integer unit time, but are very small. In all plots, data points show little variation among the 100 iterations. In all plots, data points across networks show little variation among the five graph instances

The placement of short-range edges, governed by d_{sr}, is a deterministic process, so these edges are the same in each graph instance, for a specified d_{sr}. The q long-range edges, however, are placed at random, and hence give rise to differences across graph instances.

Conditions for this evaluation are chosen so that the evacuating fraction of families is not high. For if high, then the contagion spreading reaches the looting-induced ceiling, as in Fig. 8d, and hence the variance in results will be small. This is opposite to our goal, i.e., to identify large variances. We also prefer conditions with larger numbers of long-range edges (greater q), for more variation across networks. Further, we prefer smaller $p_{e,max}$, because if $p_{e,max}$ is high (in the extreme, as $p_{e,max} \rightarrow 1$), then the evacuation contagion spread becomes deterministic. Hence, in some sense, the conditions examined here are among the worse-case conditions.

In Fig. 9, no variability in results across graph instances would be characterized by: (1) curves of different colors being horizontal—meaning no change in the fraction of families evacuating *across* graph instances, and (2) similar sizes in error bars for each data point [graph instance] of each curve—indicating the same variability in results *within* graph instances. The plots show that this is the case, and hence that results—in terms of fraction of families evaucating—do not vary significantly across graph instances.

Figure 10 shows temporal variability in simulation results, over the 10-day simulation period, rather than at the end of the 10 days, as done in the previous plots. Each curve in these plots represents a different graph instance. In Fig. 10a, data are shown for the second graph instance for the conditions $d_{sr} = 0.06$ km and $q = 16$. The variability in evacuation fraction, at each day, across the 100 runs is small; error bars, representing one standard deviation, are not visible. In Fig. 10b, these same results are again plotted along

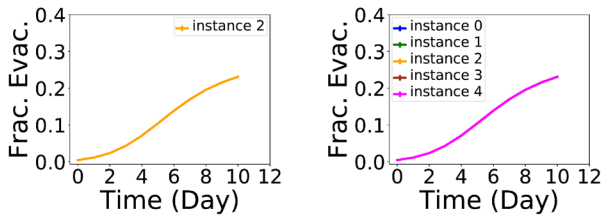

(a) $d_{sr} = 0.06$ km, $q = 16$, $p_{e,max} = 0.05$, and $n_s = 500$ **(b)** $d_{sr} = 0.06$ km, $q = 16$, $p_{e,max} = 0.05$, and $n_s = 500$

Fig. 10 Simulation results of the fraction of evacuating families (Frac. Evac.) as a function of time for different graph instances. For all curves, $d_{sr} = 0.06$ km, $q = 16$, $p_{e,max} = 0.05$, and $n_s = 500$. **a** graph instance 2. **b** graph instances 0 through 4 (5 total instances). In **b**, the data for all five graphs overlay (see instance 2 in the left plot for comparison). The variability in the form of one standard deviation is plotted as error bars for each curve, at each day. The variability in the 100 runs of one simulation (one curve) is small, and the variability across graph instances is small

with results from instances 0, 1, 3, and 4. All five curves are essentially coincident, indicating that variability across graph instances is quite small.

Based on these results illustrating minimal variance in results, further results below are given for a single graph instance.

5.3.4 Effect of dynamics model: looting 2MODE-THRESHOLD model versus classic contagion RP-THRESHOLD model

Comparisons of dynamics models Results from the 2MODE-THRESHOLD model and the RP-THRESHOLD model are compared in Fig. 11. Figure 11a through c—the top row of plots—use the 2MODE-THRESHOLD model. Figure 11a through c show the effect of probability of evacuation $p_{e,max}$ for different n_s. $p_{e,max}$ increases from 0.05 (Fig. 11a) to 0.10 (Fig. 11b) to 0.15 (Fig. 11c), with $\eta_c = 0.2$. The fraction of the population evacuating increases as n_s increases at the smallest $p_{e,max}$, almost plateaus for all n_s when $p_{e,max} = 0.1$, and increases its speed to plateau for the largest $p_{e,max}$. The values of $p_{e,max}$ were selected based survey results (Halim et al. 2020).

Figure 11d through f—the second row of plots—use the RP-THRESHOLD model, with the same values for $p_{e,max}$ and η_c. The corresponding plots stacked two-high, left to right, can be compared. As $p_{e,max}$ increases, the discrepancy between the two models increases: concern over looting dampens evacuation in the 2MODE-THRESHOLD model. For $p_{e,max} = 0.15$, the RP-THRESHOLD model results in Fig. 11f reach $f_{de} > 0.6$, while the corresponding results for 2MODE-THRESHOLD model in Fig. 11c are only roughly one-half the values of f_{de} in Fig. 11f. The 2MODE-THRESHOLD model can produce a large difference (dampening) in the fraction of families evacuating. Therefore, ignoring the influence of looting and crime can cause a large overprediction of family evacuations.

Effect of η_c in transitioning between models Figure 12 shows the effect of the range of neighbor fraction η_c over which the evacuation probability $p_{e,max}$ is non-zero. See Fig. 1a. Note that $\eta_c = 1.0$ corresponds to the RP-THRESHOLD model in Fig. 1b. In all resullts, $p_{e,max} = 0.05$ and $n_s = 300$ and in both plots, $q = 4$ and 16. Figure 12a provides results for $d_{sr} = 0.04$ km and Fig. 12b contains results for $d_{sr} = 0.1$ km. The increase in d_{sr} generates more edges (greater graph density) and more contagion spreading. The conditions of these plots were specifically chosen so that spreading was not great enough to reach the ceiling of evacuation fraction imposed by looting concerns; this limit might skew the results. Nonetheless, interestingly, the plots show that the evacuation fraction saturates by the time $\eta_c = 0.4$.

When the evacuation probability $p_{e,max}$ increases, different results are obtained. This can be seen by comparing Figs. 11c and f, where now $p_{e,max} = 0.15$. In these plots, for $\eta_c = 0.2$ and 1.0, respectively, the final fraction

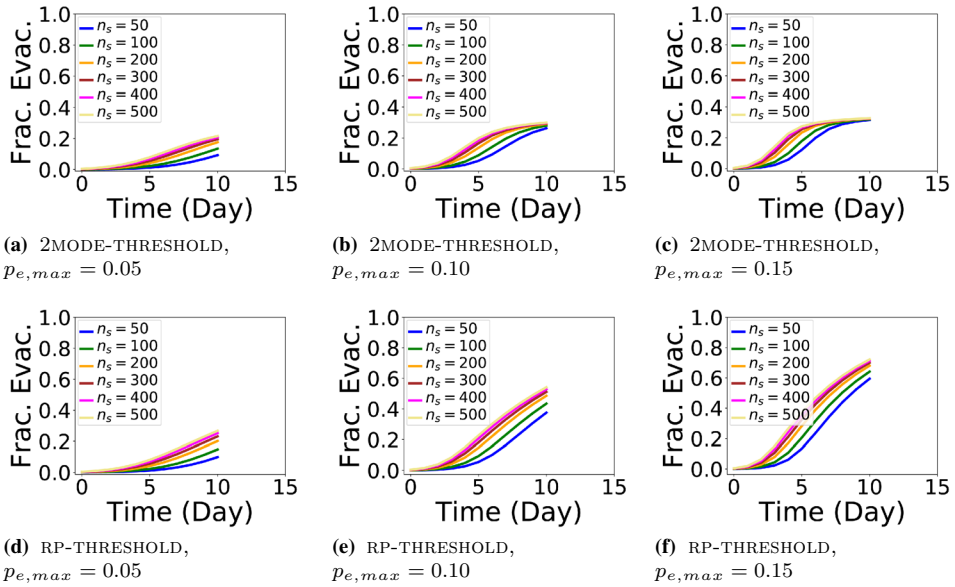

(a) 2MODE-THRESHOLD, $p_{e,max} = 0.05$ **(b)** 2MODE-THRESHOLD, $p_{e,max} = 0.10$ **(c)** 2MODE-THRESHOLD, $p_{e,max} = 0.15$

(d) RP-THRESHOLD, $p_{e,max} = 0.05$ **(e)** RP-THRESHOLD, $p_{e,max} = 0.10$ **(f)** RP-THRESHOLD, $p_{e,max} = 0.15$

Fig. 11 Simulation results of cumulative fractions of the population deciding to evacuate (Frac. Evac.) versus simulation time. Plots are arranged by row and by column. In the top row, all three results in **a** through **c** use the 2MODE-THRESHOLD model of Fig. 1a with $\eta_c = 0.2$, and n_s (numbers of random seeds) varies from 50 to 500. In the bottom row, the three results in **d** through **f** use the RP-THRESHOLD model of Fig. 1b where now $\eta_c = 1.0$, with the same n_s values. All results are for one instance of the KSW16 graph class, i.e., $q = 16$ long-range edges per node (similar results for other graph instances). All plots use $d_{sr} = 0.04$ km. By column, the left-most column (**a** and **d**) are results for $p_{e,max} = 0.05$. The middle column **b** and **e** are results for $p_{e,max} = 0.10$. The right-most column **c** and **f** are results for $p_{e,max} = 0.15$. As $p_{e,max}$ increases, the differences between the outbreak fractions for the 2MODE-THRESHOLD and RP-THRESHOLD models increase. That is, the damping effect from fear of looting becomes more pronounced. Error bars denoting one standard deviation are shown for each data point, in each curve, indicating the average results from 100 runs, but the variances are small

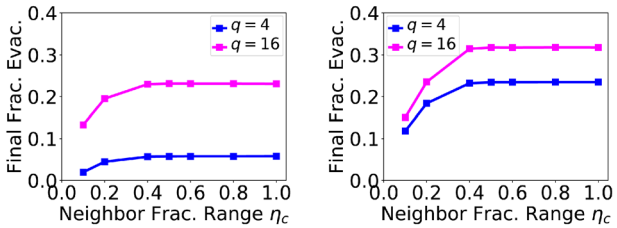

(a) $d_{sr} = 0.04$ km **(b)** $d_{sr} = 0.10$ km

Fig. 12 Simulation results of the fraction of evacuating families as a function of the range η_c where the evacuation probability $p_{e,max} > 0$ in the 2MODE-THRESHOLD model in Fig. 1a. evacuation probability $p_{e,max}$. All results use the 2MODE-THRESHOLD model of Figure 1a, $\eta_c = 0.05$ and $n_s = 300$. In **a**, $d_{sr} = 0.04$ km and $q = 4$ and 16. In **b**, $d_{sr} = 0.1$ km and $q = 4$ and 16. Number n_s of seeds is 300 in all simulations. Conditions are specifically chosen so as not to hit the upper limit in spreading due to looting, as in plots such as Fig. 11c

of evacuating families increases by 2× as η_c increases. This is a much greater increase in evacuation fraction than shown in Fig. 12, for $\eta_c = 0.2$ and 1.0, because $p_{e,max}$ has increased from 0.05 to 0.15.

5.3.5 Effect of network structure

We study the effects of long-range and short-range edges in the Virginia Beach network of 113,967 nodes.

Effect of graph structure: long-range edges The effect of q, i.e., the number of long-range edges, on the fraction of families evacuating is shown across the five plots in Fig. 13 for the 2MODE-THRESHOLD model, where $q = 0$ to 16. For $q = 0$, the fraction of the population evacuating (Frac. DE) $= f_{de} \approx 0$. This is a consequence of the networks and findings in Sect. 4. When $q = 0$, there are smaller connected components in networks (that are obviously not connected, by definition) because there are no long-range edges. As a result, contagion cannot move from one component to another. As q increases to 2 and then to 16 long-range edges per node, f_{de} increases markedly. In particular, Fig. 13e shows how the spread of evacuation decisions has an upper bound in the 2MODE-THRESHOLD model: too many families have evacuated, so the remaining families do not evacuate over concerns of looting and crime. This behavior is also seen for $q = 8$, and to a lesser extent, for $q = 4$ when $n_s = 500$. This effect of greater contagion spreading as q increases is the "weak link" phonemena (Granovetter 1973), where long-range edges can cause remote nodes to change their state to 1 (i.e., evacuating), thus moving a "contagion"

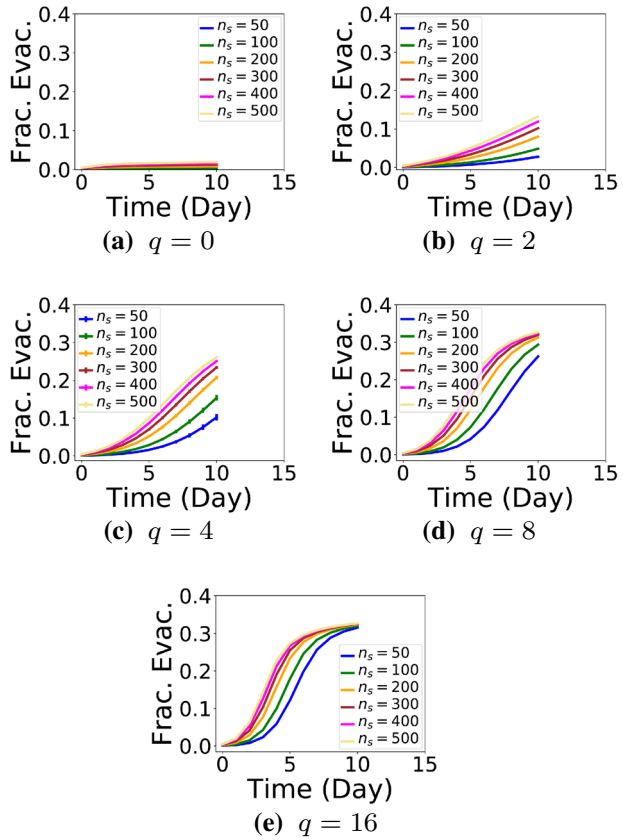

Fig. 13 Simulation results of fraction of evacuating families (Frac. Evac.) versus simulation time. The plots also show the effects of q, i.e. the number of long-range edges, and numbers of seed nodes. Each plot has curves for a different q, from 0 through 16. All results use the 2MODE-THRESHOLD model of Figure 1a, $p_{e,max} = 0.15$, $\eta_c = 0.2$, and n_s (numbers of random seeds) varies from 50 to 500 (see legend). Error bars denote variance across the 100 runs that are used to generate each curve in each plot. (The variance is very small.) Results for one graph instance of each of the following graphs: **a** KSW0, **b** KSW2, **c** KSW4, **d** KSW8, and **e** KSW16, where each graph class is of the form KSWq. In all plots, $d_{sr} = 0.04$ km. As q increases, the fraction of families evacuating increases, up to the point that the looting mechanism constrains further evacuation

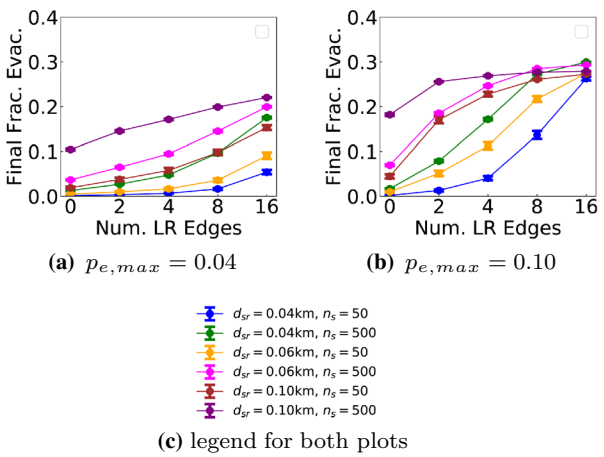

Fig. 14 Simulation results of the fraction of evacuating families (Frac. Evac.) as a function of the number q of long-range (LR) edges. All results use the 2MODE-THRESHOLD model of Fig. 1a, $\eta_c = 0.2$, and n_s (numbers of random seeds) is 50 and 500 (see legend). Error bars denote standard deviation. (The variance is very small.) Results are for one graph instance, instance 0, for each d_{sr} value (0.04 km, 0.06 km, 0.10 km). The maximum probability in the 2MODE-THRESHOLD is **a** $p_{e,max} = 0.04$ and **b** $p_{e,max} = 0.10$. The results show that increasing $p_{e,max}$ by 2.5× results in increases in f_{de}, particularly at larger q. The increases are limited by the maximum evacuation fraction of about 0.3. **c** Legend for both plots

into a different region of a graph. Note that the speed with which the maximum of $f_{de} = 0.32$ is attained increases with n_s.

From Table 1, the average in-degree for a node in KSW0 for $d_{sr} = 40$m is 10.1. The average in-degree increases by about 70% to 17.7 for KSW8, and this increase is due solely to the long-range edges. Hence, this figure shows that by the time the average in-degree of the graphs for $d_{sr} = 40$m increases by 70% owing to long-range edges, the effect of looting, in plateauing the fraction of families evacuating, is observed.

Figure 14 provides the fraction f_{de} of evacuating families as a function of number of long-range edges for all three d_{sr} values—0.04 km, 0.06 km, and 0.1 km—for two numbers n_s of seed nodes: 50 and 500. The two plots are, for left, $p_{e,max} = 0.04$ and, for right, $p_{e,max} = 0.10$ in the 2MODE-THRESHOLD model of Fig. 1a. Across both plots, f_{de} increases as q increases, but also as d_{sr}, n_s, and $p_{e,max}$ increase. A couple of observations about the looting model are relevant, but will return to these issues when the appropriate simulation input is the focus.

Effect of graph structure: short-range edges Figure 15 shows the effect of short-range distance d_{sr} on the evacuation fraction. For the smallest d_{sr}, there is an effect of q on the fraction of evacuating families. However, by the time d_{sr} reaches its greatest value, the number of short-range edges grows such that for all $q \geq 2$, the evacuation fraction is approaching its maximum value. In this way, increases in either d_{sr} or q has the same net effect: increases in either increases the number of edges in a graph (i.e., increases the graph density) and hence increases the diffusion of evacuation up to the looting-imposed ceiling.

5.3.6 Effects of model parameter $p_{e,max}$.

Figure 14, described above, shows the effect of increasing $p_{e,max}$ on increasing f_{de} values. First, note that for $p_{e,max} = 0.10$, according to Table 5, roughly 0.65 fraction of the families should be evacuating. But because of the concern over looting, f_{de} is far less (about 1/2 of the value)

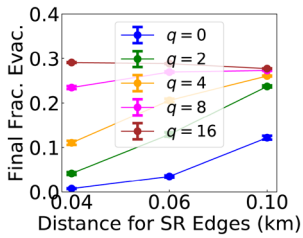

Fig. 15 Simulation results of the fraction of evacuating families (Frac. Evac.) as a function of the short-range (SR) distance d_{sr} over which SR edges are formed between pairs of families. All results use the 2MODE-THRESHOLD model of Figure 1a, $\eta_c = 0.2$, $p_{e,max} = 0.05$, $n_s = 200$, and all q values (see legend). Error bars denote standard deviation from 100 runs. (The variance is very small.) Results are for one graph instance, instance 0, for each d_{sr} value (0.04 km, 0.06 km, 0.10 km). The results show that for $d_{sr} = 0.04$ km, there is a pronounced effect of q. However, as d_{sr} increases, the number of short-range edges increases, giving more opportunities for contagion to spread, and by the time $d_{sr} = 0.10$ km, the effect of different $q \geq 2$ is small, as the spread of evacuation approaches its limit value

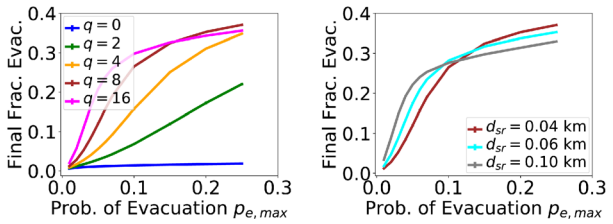

(a) $d_{sr} = 0.04$ km **(b)** $q = 8$

Fig. 16 Simulation results of the final fraction of families deciding to evacuate (Frac. Evac.) as a function of the evacuation probability $p_{e,max}$. All results use the 2MODE-THRESHOLD model of Figure 1a, $\eta_c = 0.2$ and $n_s = 400$. In **a**, the different curves are for different numbers q of long-range edges, with $d_{sr} = 0.04$ km. In **b**, the different curves are for d_{sr} values of 0.04 km, 0.06 km, and 0.10 km, for $q = 8$. For reference, the brown curve for $d_{sr} = 0.04$ km and $q = 8$ is the same in both plots. Error bars, denoting one standard deviation, are plotted, but variance is very small. The transitions observed in the plots (i.e., intersections of curves) are caused by greater $p_{e,max}$ and greater degree networks (large d_{sr}, large q). In these cases, the fast and widespread diffusion of contagion can result in nodes in state 0 having more than $\eta_c = 0.2$ fractions of their neighbors in state 1, and for the 2MODE-THRESHOLD model, this means that the nodes will not transition to state 1. This means that the overall spread size may be less

in Fig. 14b. This same type of comparison is also provided in Fig. 11.

Second, Fig. 14a is a sufficiently small $p_{e,max} = 0.04$ that the overall spread fraction f_{de} is not greater than about 0.2, which is η_c in Fig. 1a. Consequently, looting does not have a big effect on these results. However, for the larger $p_{e,max} = 0.10$ in Fig. 14b, some of the curves plateau at greater q, particularly for $d_{sr} = 0.1$ km and $n_s = 500$, but also to a lesser extent when either $d_{sr} = 0.1$ km or $n_s = 500$. These curves are reaching a ceiling, indicating that the looting factor is having an effect. Hence, the looting phenomenon may or may not be operative when using the 2MODE-THRESHOLD model: in Figure 14, this is controlled by $p_{e,max}$.

5.3.7 Effects of model parameters $p_{e,max}$ and η_c Combined with Network Structure.

Figure 16 shows the explicit dependence of the final fraction of families evacuating (Final Frac. Evac. in plots) as a function of the evacuation probability $p_{e,max}$ of the 2MODE-THRESHOLD model of Fig. 1a. The number n_s of seeds is 400 in all simulations. Figure 16a fixes $d_{sr} = 0.04$ km and varies the number q of long-range edges, while Fig. 16b fixes $q = 8$ and varies d_{sr}. In the left plot, for fixed d_{sr}, the spread fraction increases as $p_{e,max}$ and q increase. However, for larger q of 2, 4, 8, and 16, and for larger $p_{e,max}$, the largest $q = 16$ produces a shallower rate of increase in f_{de} than do the other q values. Similarly in right plot, as d_{sr} increases for fixed $q = 8$, as $p_{e,max}$ increases, there is a transition in ranking of the short-range distance d_{sr} that causes larger outbreaks. The transition occurs near $p_{e,max} = 0.1$.

In both aforementioned plots, the same mechanism is operative. When the probability $p_{e,max}$ increases to larger values (roughly for $p_{e,max} > 0.1$ for these plots) and when average in- and out-degrees are large (roughly for $d_{min} = d_{max} \geq 20$), the spreading is fast. We can conceptualize a "frontal boundary" that separates nodes in state 0 from those in state 1. As a contagion grows, the frontal boundary of state 1 pushes into parts of the network where nodes are in state 0. For greater $p_{e,max}$ and greater degree, the front can be widespread so that nodes in state 0 can have fractions of neighbors in state 1 that are greater than $\eta_c = 0.2$, in which case these nodes will not transition to state 1, per Fig. 1a. This means that the overall spread fraction is less than what might otherwise be anticipated.

Thus, dynamics model parameters and network structure combine to produce two interesting phenomena. First, as $p_{e,max}$ increases, the *rate* of increase in the *final* fraction of evacuating families can *decrease*. Second, as $p_{e,max}$ increases, the *magnitude* of the *final* fraction of evacuating families can *decrease*.

5.3.8 Effects of numbers of seed nodes

Figure 17 provides the final fraction of families evacuating as a function of numbers n_s of seed families (that are evacuating at time $t = 0$). The effect of numbers of seeds—like all parameters—is dependent on the regime of final evacuation fraction that the conditions produce. When conditions are such that the evacuation fraction is less than the looting-induced evacuation fraction ceiling, then the effect of seed nodes can be significant; see the curve for $q = 4$. However,

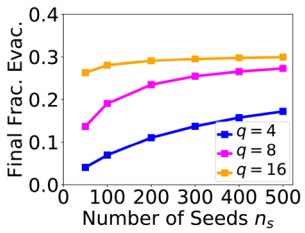

Fig. 17 Simulation results of the final fraction of evacuating families as a function of the number n_s of seed families (i.e., the number of families evacuating at time $t = 0$). Conditions are $d_{sr} = 0.04$ km, $q = 4$, 8, and 16, $\eta_c = 0.2$, and $p_{e,max} = 0.10$ in the 2MODE-THRESHOLD model in Figure 1a. The results show that for conditions in which the evacuation fraction looting-induced ceiling is not reached (here, for $q = 4$), a 10 fold increase in n_s from 50 to 500, can produce a fourfold increase in final evacuation fraction (from 0.035 to 0.15 probability). As final evacuation fraction increases such that the looting-based ceiling is reached (here, for $q = 16$), the effect of seed nodes is minimal

when the looting ceiling is reached, which for these conditions occurs when $q = 16$, the effect of seed nodes is small.

6 Related work

6.1 Factors affecting evacuation decision

Many studies have identified factors that affect evacuation decision-making. These include social networks, peer influence, access to resources, risk perceptions (Riad et al. 1999; Lindell and Perry 2005; Dash and Gladwin 2007) and household demographics such as nationality, proximity to hurricane path, pets, disabled family members, mobile home, access to a vehicle, etc. (Baker 1991, 1995; Fu and Wilmot 2004a; Dash and Gladwin 2007; Widener et al. 2013; Burnside 2006; Cole and Fellows 2008; Faucon 2010; Wong et al. 2018). Evacuation notices can increase people's propensity to evacuate (Baker 1991, 1995; Dash and Gladwin 2007; O'Neil 2014). Mozumder and Vásquez (2015) provide a case study in which they analyze the role of evacuation expenses in affecting hurricane evacuation decisions in Harris and Galveston counties in Texas. Studies also show the importance of storm characteristics into evacuation decision-making (Baker 1991, 1995; Dash and Gladwin 2007; Mozumder and Vásquez 2018).

Work by Goldberg et al. shows that a family's past decision to evacuate (or not) is a significant predictor of a similar future intended evacuation behavior if the family had a high confidence in its past decision (Goldberg et al. 2020). Role of strong social ties in evacuation behavior is studied in Metaxa-Kakavouli et al. (2018). Authors show several aspects of social capital are correlated with evacuation decision, even after accounting for confounding factors. Especially, higher levels of bridging and linking social ties correlate strongly with evacuation. Miller (2007) examines the role of formal and informal social connections in sharing information and shows that the number of contacts as well as the range of contacts across different contexts (e.g., faith-based, school, work, etc.) aided evacuation during hurricanes Katrina and Rita in East Texas. Influence of density, diversity, and dependability of social support and social connections is studied on decisions to evacuate in Collins et al. (2018).

6.2 Agent-based modeling and simulation of evacuation decision-making

Some studies use social networks and relative threshold models to model evacuation behavior. A *relative threshold* θ_i for agent v_i is the minimum fraction of distance-1 neighbors in a social network $G(V, E)$ that must be in state 1 in order for v_i to change from state 0 and to state 1 (Watts 2002; Centola and Macy 2007). Several studies (Hasan and Ukkusuri 2011; Widener et al. 2013; Yang et al. 2019) assign thresholds to agents in agent-based models (ABMs) of hurricane evacuation modeling. Stylized networks of 2000 nodes are used in Hasan and Ukkusuri (2011) to study analytical and ABM solutions to evacuation. In Widener et al. (2013), 12,892 families are included in a model of a 1995 hurricane for which 75% of households evacuated. They include three demographic factors in their evacuation model, in addition to the peer influence that is captured by a threshold model. Small world and random regular stylized networks are used for social networks.

Dixon et al. (2017) provide a survey-based empirical analysis for identifying the most salient factors of the heterogeneous respondents, which inform the rules governing hurricane evacuation behavior of the subpopulations in an agent-based model. Kuhlman et al. (2020) develop an agent-based model for evacuation decision-making from Hurricane Sandy survey data.

Simulations of hurricane evacuation decision-making in the Florida Keys are presented in Yang et al. (2019). The simulations cover 24 h, where the actual evacuation rate was about 53%. The social network is a small-world network, with geospatial home locations, which is similar to our network construction method. Edges between homes are placed by using a small world approach (Watts and Strogatz 1998); long range edges are placed by travel times. The dynamics of evacuation is modeled as a two-step process. First, families receive a message to evacuate either directly, or via diffusion through the social network and then families evacuate based on a relative threshold, i.e., the fraction of a family's neighbors that have decided to evacuate.

In all of these studies, except Kuhlman et al. (2020), as the number of neighbors of a family v_i evacuates, the more likely it is that v_i will evacuate. Our threshold model differs:

in our model, if too many neighbors evacuate, then v_i will not evacuate because of concerns over crime and looting.

ABM requires a representation of a population. Two studies use synthetic population (i.e., digital twin Barrett et al. (2009)) data to represent a population; they use the US census data, a commercial data set of business locations, Census Transportation Planning Products, and other data to produce families and then use stylized methods to form edges of the social networks (Widener et al. 2013; Yang et al. 2019). These approaches are similar to our work. Works using stylized networks include Hasan and Ukkusuri (2011); Yang et al. (2019).

Yin et al. (2014) study not only evacuation decision-making, but also destination selection for evacuation and travel planning, for Miami-Dade County. They make use of data from several surveys to develop models. Zhu et al. (2018) also combine survey data with synthetic data to develop an ABM for evacuation decision-making, and for travel of families that are evacuating. They model Hurricane Sandy and four million families in the northeastern US.

6.3 Other modeling approaches

Some studies predict human evacuation behavior using techniques other than ABM. Social media data have been used to model hurricane evacuation decision-making and travel patterns. Roy and Hasan (2021) construct an input-output hidden Markov model to predict hurricane evacuations using Twitter data. Roy et al. (2021) use social media data to predict traffic demand based on evacuations in the face of oncoming hurricanes. Fu and Wilmot (2004b) build a sequential binary logit model to compute the probability that households evacuate at each time step as a hurricane approaches land.

7 Summary and conclusions

We study evacuation decision-making as a graph dynamical system using 2MODE-THRESHOLD functions for nodes. This work is motivated by the results of a survey collected during Hurricane Sandy which shows that concerns about crime motivates families to stay in their homes, if too many neighbors evacuate. We study the dynamics of 2MODE-THRESHOLD in different network settings, and show significant differences from the standard threshold model. The result shows that in some cases, not incorporating the looting effect in the model can overpredict evacuation rates by as much as 50%. This has important policy implications. For example, a more realistic prediction of the size of non-evacuees can be used by city planners for contingency planning. Planners can more accurately estimate resources that will be required for non-evacuees who are left behind in adverse conditions, as well as design interventions that will address the concerns of crime so that a higher level of compliance to evacuation may be achieved.

Acknowledgements This work has been partially supported by the following grants: NSF CRISP 2.0 Grants 1916670 and 1832693, NSF OAC-1916805 (CINES), DTRA CNIMS (Contract HDTRA1-11-D-0016-0001), NSF DIBBS Grant ACI-1443054, NSF EAGER Grants CMMI-1745207 and SAI-2122135, and NSF BIG DATA Grant IIS-1633028.

References

Adiga A, Kuhlman CJ, Marathe MV, Mortveit HS, Ravi SS, Vullikanti A (2018) Graphical dynamical systems and their applications to bio-social systems. Int J Adv Eng Sci Appl Math 1–19

Ahmed NK, Alo RA, Amelink CT, Baek YY, Chaudhary A, Collins K, Esterline AC, Fox EA, Fox GC, Hagberg A, Kenyon R, Kuhlman CJ, Leskovec J, Machi D, Marathe MV, Meghanathan N, Miyazaki Y, Qiu J, Ramakrishnan N, Ravi SS, Rossi RA, Sosic R, von Laszewski G (2020) net.science: a cyberinfrastructure for sustained innovation in network science and engineering. In: Proceedings of the gateways 2020 conference (science gateways community institute), p 4

Akerlof GA, Romer PM, Hall RE (1993) Mankiw NG (1993) Looting: The economic underworld of bankruptcy for profit. Brook Papers Econ Activ 2:1–73

Aral S, Nicolaides C (2017) Exercise contagion in a global social network. Nat Commun 8:14753

Azam JP (2002) Looting and conflict between ethno-regional groups: Lessons for state formation in Africa. J Conflict Resol 46(1):131–153

Baker EJ (1991) Evacuation behavior in hurricanes. Int J Mass Emerg Disas 9(2):287–310

Baker EJ (1995) Public responses to hurricane probability forecasts. Prof Geograph 47(2):137–147

Barrett CL, Beckman RJ, et al. (2009) Generation and analysis of large synthetic social contact networks. In: Winter simulation conference, pp 1003–1014

Beckman R, Kuhlman C et al (2011) Modeling the spread of smoking in adolescent social networks. In: Proceedings of the fall research conference of the association for public policy analysis and management, Citeseer

Burnside R (2006) Leaving the big easy: an examination of the hurricane evacuation behavior of new orleans residents before hurricane katrina. J Public Manage Social Policy 12:49–61

Centola D (2010) The spread of behavior in an online social network experiment. Science 329:1194–1197

Centola D (2011) An experimental study of homophily in the adoption of health behavior. Science 334:1269–1272

Centola D, Macy M (2007) Complex contagions and the weakness of long ties. Am J Sociol 113(3):702–734

Chen J, Lewis B et al (2017) Individual and collective behavior in public health epidemiology. In: Handbook of statistics, vol 36, Elsevier, pp 329–365

Cole TW, Fellows KL (2008) Risk communication failure: a case study of new orleans and hurricane katrina. Southern Commun J 73(3):211–228

Collins J, Ersing RL, Polen A, Saunders M (2018) Evacuation Behavior Measured During an Evacuation Order: an assessment of the effects of social connections on the decision to evacuate. Nat Haz Center

Coumou D, Rahmstorf S (2012) A decade of weather extremes. Nat Clim Change 2:491–496
Dash N, Gladwin H (2007) Evacuation decision making and behavioral responses: individual and household. Nat Haz Rev 8(3):69–77
Dixon D, Mozumder P, Vásquez WF, Gladwin H (2017) Heterogeneity within and across households in hurricane evacuation response. Netw Spatial Econ 17(1):1–36
Dubhashi DP, Panconesi A (2009) Concentration of measure for the analysis of randomized algorithms. Cambridge University Press, Cambridge
Dynes RR, Quarantelli EL (1968) What looting in civil disturbances really means. Transaction 5(6):9–14
Erskine H (1974) The polls: fear of violence and crime. Public Opin Quarterly 38(1):131–145
Faucon C (2010) The suspension theory: Hurricane katrina looting, property rights, and personhood. Louisiana Law Rev 70(4):1303–1338
Ferris T et al (2016) Studying the usage of social media and mobile technology during extreme events and their implications for evacuation decisions: A case study of hurricane sandy. Int J of Mass Emerg Dis 34(2):204–230
Fu H, Wilmot CG (2004) Sequential logit dynamic travel demand model for hurricane evacuation. Transp Res Part B 45:19–26
Fu H (1882) Wilmot CG (2004b) Sequential logit dynamic travel demand model for hurricane evacuation. Transp Res Record 1:19–26. https://doi.org/10.3141/1882-03
Goldberg MH, Marlon JR, Rosenthal SA, Leiserowitz A (2020) A meta-cognitive approach to predicting hurricane evacuation behavior. Environ Commun 14(1):6–12
Gonzalez-Bailon S, Borge-Holthoefer J, Rivero A, Moreno Y (2011) The dynamics of protest recruitment through an online network. Nat Sci Rep 1–7. https://doi.org/10.1038/srep00197
Granovetter M (1973) The strength of weak ties. Am J Sociol 78(6):1360–1380
Granovetter M (1978) Threshold models of collective behavior. Am J Sociol 83(6):1420–1443
Hagberg AA, Schult DA, Swart PJ (2008) Exploring network structure, dynamics, and function using NetworkX. In: Proceedings of the 7th python in science conference (SciPy2008), pp 11–15
Halim N, Mozumder P (2020) Factors influencing evacuation behavior during Hurricane sandy. Risk analysis (to be submitted)
Halim N, Kuhlman CJ, Marathe A, Mozumder P, Vullikanti A (2020) Two-mode threshold graph dynamical systems for modeling evacuation decision-making during disaster events. In: Cherifi H, Gaito S, Mendes JF, Moro E, Rocha LM (eds) Complex networks and their applications VIII. Springer International Publishing, pp 519–531
Hasan S, Ukkusuri SV (2011) A threshold model of social contagion process for evacuation decision making. Transp Res Part B 45:1590–1605
Kempe D, Kleinberg J, Tardos E (2003) Maximizing the spread of influence through a social network. In: Proceedings of ACM KDD, pp 137–146
Kleinberg J (1999) The small-world phenomenon: an algorithmic perspective. Technical Report 99-1776
Kuhlman C, Marathe A, Vullikanti A, Halim N, Mozumder P (2020) Increasing evacuation during disaster events. In: AAMAS, pp 654–662
Kumar H (2019) Cyclone fani hits india: storm lashes coast with hurricane strength. New York Times
Leskovec J, Sosič R (2016) SNAP: a general-purpose network analysis and graph-mining library. ACM Trans Intell Syst Technol 8(1):1
Lindell MK, Perry RW (2005) Warning mechanisms in emergency response systems. Int J Mass Emerg Disast 5(2):137–153
Madireddy M, Tirupatikumara S et al (2015) Leveraging social networks for efficient hurricane evacuation. Transp Res Ser B Methodol 77:199–212
Meng S, Mozumder P (2020) Hurricane sandy: damages, disruptions and pathways to recovery. Risk analysis (under review)
Metaxa-Kakavouli D, Maas P, Aldrich DP (2018) How social ties influence hurricane evacuation behavior. In: Proceedings of the ACM on human-computer interaction 2(CSCW), pp 1–16
Miller LM (2007) Collective disaster responses to katrina and rita: exploring therapeutic community, social capital, and social control. J Rural Social Sci 22(2):4
Mortveit H, Reidys C (2007) An introduction to sequential dynamical systems. Springer, Berlin
Mozumder P, Vásquez WF (2015) An empirical analysis of hurricane evacuation expenditures. Nat Haz 79(1):81–92
Mozumder P, Vásquez WF (2018) Understanding hurricane evacuation decisions: a stated preference approach. Environ Resour Econ 71(2):407–425
Nguyen VT (2018) Thee displaced: refugee writers on refugee lives. Abrams, New York, NY
O'Neil PD (2014) Emergency evacuation orders: considerations and lessons from hurricane sandy. J Emerg Manage 219–227
Riad JK, Norris FH, Ruback RB (1999) Predicting evacuation in two major disasters: risk perception, social influence, and access to resources. J Appl Social Psychol 20(5):918–934
Romero D, Meeder B, Kleinberg J (2011) Differences in the mechanics of information diffusion. In: Proceedings of the 20th international world wide web conference (WWW)
Roy KC, Hasan S (2021) Modeling the dynamics of hurricane evacuation decisions from twitter data: an input output hidden markov modeling approach. Transp Res Part C Emerg Techno 123:1–16
Roy KC, Hasan S, Culotta A, Eluru N (2021) Predicting traffic demand during hurricane evacuation using real-time data from transportation systems and social media. Transp Res Part C 1–16
Saunders M, Lea A (2020) August forecast update for north atlantic hurricane activity in 2020. Technical report. http://www.tropicalstormrisk.com/docs/TSRATLForecastAug2020.pdf, tropical Risk Forecast.com
Schelling TC (2006) Micromotives and macrobehavio, revised. W. W. Norton & Company
Sengupta S (2019) Extreme weather displaced a record 7 million in first half of 2019. New York Times
Watts D (2002) A simple model of global cascades on random networks. PNAS 99:5766–5771
Watts DJ, Strogatz SH (1998) Collective dynamics of 'Small-World' networks. Nature 393:440–442
Widener MJ, Horner MW et al (2013) Simulating the effects of social networks on a population's hurricane evacuation participation. J Geogr Syst 15:193–209
Wong S, Shaheen S, Walker J (2018) Understanding evacuee behavior: a case study of Hurricane Irma. Technical report. https://escholarship.org/uc/item/9370z127
Yang Y, Mao L, Metcalf SS (2019) Diffusion of hurricane evacuation behavior through a home-workplace social network: a spatially explicit agent-based simulation model. Comput Environ Urban Syst 74:13–22
Yin W, Murray-Tuite P, Ukkusuri SV, Gladwin H (2014) An agent-based modeling system for travel demand simulation for hurricane evacuation. Transp Res Part C Emerg Technol 42:44–59
Zhu Y, Xie K, Ozbay K, Yang H (2018) Hurricane evacuation modeling using behavior models and scenario-driven agent-based simulations. Proc Comput Sci 130:836–843